

Effects of equilibrium coexisting phases in the first-order chiral transition within the Linear sigma model with quarks

R. M. Aguirre

*Departamento de Matematica,
Universidad Nacional de La Plata
and Instituto de Fisica La Plata, CONICET
Argentina*

The first order chiral phase transition for quark matter with flavor imbalance is studied using the Linear sigma model with quarks, also known as Quark-meson model. Special attention is paid to the role of the scalar isovector meson. The general consensus presently is that the chiral transition changes from a smooth crossover to first-order at low temperatures. This transition is assumed to be discontinuous, with unstable or metastable intermediate states. However, if multiple charges are simultaneously conserved the system could undergo a continuous change through a coexistence of equilibrium states. Under such assumption the bulk properties are analyzed and several remarkable effects for the speed of sound and the susceptibilities are stressed.

I. INTRODUCTION

The gross features of the QCD phase diagram have been deduced long time ago, however the precise details are still pending. Intensive investigations on strong interacting matter under extreme conditions of density and temperature have scrutinized the different regimes, providing information on new aspects. Experiments on heavy ion collisions, for instance, have provided a lot of evidence to understand the high temperature and low matter concentration domain. On the other hand, the observation of compact astronomical objects permanently produce new data which is elaborated to understand the low temperature and medium-high density regime. Additional precisions have been obtained from the lattice simulation of the fundamental theory (LQCD) [1–4]. This method is particularly appropriate to study the vacuum properties and finite temperature effects, although finite density systems are not accessible due to the well known problem of the negative sign. To avoid this technical difficulty the study of matter at zero baryon density but with isospin imbalance, has been proposed [1]. The conservation of the isospin charge, with the introduction of the corresponding chemical potential μ_I , eliminates the problem of the determinant.

Complementarily, the regime of medium-high baryon densities and low temperatures is commonly analyzed using effective models since first principle calculations, as in lattice simulations, are not feasible. Several theoretical models highlighting different aspects of the strong interaction have been used. The compilation of their predictions has produced a complex picture of the phase diagram, with diverse phase transitions, condensates, collective states, etc.

Due to the property of asymptotic freedom of the QCD theory, it has been hypothesized that an state of deconfined quarks and gluons could be obtained under extreme conditions. This deconfinement phase transition has particularly been analyzed [5, 6] since it could have clear manifestations in heavy ion collision events or, as pointed out more recently, it could leave its imprint in the gravitational waves coming from the collapse of companion neutron stars.

The recovery of the chiral symmetry is also expected to occur through a phase transition following a pattern similar to the deconfinement case. A change of character from first-order at low temperatures to second order at higher ones is expected. If the quarks have a non-zero mass, the second order transition becomes a soft crossover. In any case the line of transition points in the (μ_B, T) plane exhibits a critical endpoint (CEP) separating different regimes.

General features of the chiral transition in quark matter with isospin imbalance have been investigated in [7–28]. The coherence of the theoretical predictions with the LQCD results at zero baryon number has been particularly analyzed in [11, 22–24, 28].

It has been argued that in the limit of zero baryonic density ($\mu_B = 0$) at constant isospin fraction, the associated chemical potential μ_I can be treated as a gauge field [2]. Under this hypothesis the pion field could experience a condensation along the chiral transition. However, it has been pointed out that a system with $\mu_I > \mu_B$ could be unstable by weak decay.

The fluctuations of conserved charges are good markers of the phase transitions, being related to the corresponding thermodynamical susceptibilities by the fluctuation dissipation theorem [29]. For this reason the susceptibilities associated with the baryonic number or electric charge, have been focused by the LQCD. Furthermore, they provide local information of the equation of state.

The aim of this paper is the study of the phase diagram near the chiral transition, by taking the quark number density and the temperature as thermodynamical variables and considering the conservation of the isospin asymmetry. The Linear Sigma Model with quarks (LSMq) is specially suited for this purpose, as it was originally conceived to reproduce the low energy phenomenology of QCD. The weak interaction is not considered here, as it is a common

practice [2]. Therefore, the u and d quark flavors are stable degrees of freedom. Furthermore, an scalar isovector meson ζ is introduced and treated on the same foot as the standard σ, π ones. This field propagates the flavour interaction between quarks. An enlarged family of mesons within the LSMq have been considered previously [30–32], and particularly the role of the ζ meson [18, 33–37]. In order to stress the results on thermodynamical instabilities, the simplicity of the theoretical formulation is preferred here. Hence, only the meson fields σ, π, ζ and the Hartree approach are considered here, to take advantage of the simplicity and versatility of the model. Notwithstanding a more sophisticated approach is in progress.

The rest of this work is organized as follows, the mean field approach to the LSMq, also known as Quark Meson model, is presented in the next section. The results for the thermodynamics of the system is discussed in Sec. III, and the final conclusions are drawn in Sec. IV.

II. THE MODEL

The simplest version of the LSMq, with the only addition of the ζ meson, can be written as [37]

$$\begin{aligned} \mathcal{L} = & \bar{\Psi} (i \not{\partial} + g \Phi) \Psi + \frac{1}{2} (\partial_\mu \sigma \partial^\mu \sigma + \partial_\mu \boldsymbol{\pi} \cdot \partial^\mu \boldsymbol{\pi} + \partial_\mu \boldsymbol{\zeta} \cdot \partial^\mu \boldsymbol{\zeta}) + \frac{1}{4} C_0 \text{Tr} (\Phi^\dagger \Phi) \\ & - \frac{1}{16} C_3 [\text{Tr} (\Phi^\dagger \Phi)]^2 - \frac{1}{8} C_2 \text{Tr} (\Phi^\dagger \Phi)^2 - h \sigma \end{aligned} \quad (1)$$

the two quark flavors are collected in the bi-spinor $\Psi = (\psi_u \psi_d)^t$, the meson σ and the iso-multiplets scalar $\boldsymbol{\zeta}$, and pseudo-scalar $\boldsymbol{\pi}$, constitute $\Phi = \sigma + i \gamma_5 \boldsymbol{\pi} \cdot \boldsymbol{\tau} + \boldsymbol{\zeta} \cdot \boldsymbol{\tau}$. Flavor degeneracy in the quark coupling is assumed and a symmetry breaking term, linear in σ has been included.

The scalar meson fields can be decomposed as the sum of a thermal expectation value and its fluctuation $\sigma = s + \delta\sigma$, $\zeta_a = z \delta_{a3} + \delta\zeta_a$. The quark fields acquire finite masses at the tree level, as can be easily seen after the expansion in the meson fluctuations and examining terms proportional to $\bar{\psi}_j \psi_j$. Thus, the effective quark mass $m_j = g(s + I_j z)$ can be identified, where $I_j = 1 (-1)$ for $j = u (d)$. By the same procedure, but collecting quadratic terms in the meson fluctuations $\delta\sigma^2, \delta\zeta_a^2, \pi_a^2$, one can identify the meson masses [35]

$$M_\sigma^2 = -C_0 + 3C_3 s^2 + (C_3 + 2C_2) z^2, \quad M_{\pi_a}^2 = -C_0 + C_3 (s^2 + z^2), \quad M_{\zeta_a}^2 = -C_0 + C_3 n_a z^2 + (C_3 + 2C_2) s^2 \quad (2)$$

with $n_a = 1 (3)$ for $a = 1, 2 (3)$.

The mean field approach (MFA) is obtained when the meson fluctuations are completely omitted, while its explicit consideration can be arranged as higher order corrections [38–40]. Here I adopt the Hartree approach, which consist of the MFA complemented with the vacuum contribution from the Dirac sea of quarks. The MFA is the standard approach in quark matter calculations using the effective Nambu-Jona Lasinio model [41–43], and it has been used in the case of the LSMq model too [36, 44]. An equivalent treatment is usual in relativistic hadronic models, and it is applied to study phase transitions as the nuclear liquid-gas, or the quark deconfinement in high density matter [45].

Within the Hartree scheme the grand potential per unit volume of uniform quark matter can be written as

$$\omega(T, \mu) = \omega_{\text{vac}} - \frac{N_c}{\beta\pi^2} \sum_{j=u,d} \int_0^\infty dp p^2 \left[\log \left(1 + e^{-\beta(E_{pj} - \mu_j)} \right) + \log \left(1 + e^{-\beta(E_{pj} + \mu_j)} \right) \right] \quad (3)$$

where

$$E_{pj} = \sqrt{p^2 + g^2 (s + I_j z)^2}, \quad I_j = 1, -1 \text{ for } j = u, d \quad (4)$$

The vacuum term is divergent, but a finite contribution can be extracted by dimensional regularization followed by an appropriate subtraction scheme, as shown in the Appendix

$$\omega_{\text{vac}} = \frac{N_c}{8\pi^2} \sum_{j=u,d} \left[m_j^4 \log \left(\frac{m_j}{m_0} \right) + \frac{m_0^4 - m_j^4}{4} \right] \quad (5)$$

Here m_0 stands for the degenerate mass physical value.

As usual, the definition of the mean values s, z are given by the stationary conditions

$$0 = \frac{\partial \omega}{\partial s}, \quad 0 = \frac{\partial \omega}{\partial z},$$

which lead to the equations

$$0 = (-C_0 + C_3 s^2 + C_4 z^2) s - h - \frac{gN_c}{\pi^2} \sum_{j=u,d} m_j \left[\frac{m_j^2}{2} \log \left(\frac{m_j}{m_0} \right) - \int_0^\infty \frac{dp p^2}{E_j} (n_{Fj} + \bar{n}_{Fj}) \right], \quad (6)$$

$$0 = (-C_0 + C_3 z^2 + C_4 s^2) z - \frac{gN_c}{\pi^2} \sum_{j=u,d} I_j m_j \left[\frac{m_j^2}{2} \log \left(\frac{m_j}{m_0} \right) - \int_0^\infty \frac{dp p^2}{E_j} (n_{Fj} + \bar{n}_{Fj}) \right], \quad (7)$$

respectively. In Eqs.(6, 7) the equilibrium Fermi distribution functions $n_{Fj}(T, \mu_j)$ for quarks and $\bar{n}_{Fj}(T, \mu_j)$ for antiquarks have been introduced.

The entropy of the system is given by the thermodynamical definition $\mathcal{S} = S/V = -\partial\omega/\partial T$ as

$$\mathcal{S}(T, \mu) = -\frac{\omega - \omega_{\text{vac}}}{T} + \frac{N_c}{\pi^2 T} \sum_{j=u,d} \int_0^\infty dp p^2 [(E_j - \mu_j) n_{Fj} + (E_j + \mu_j) \bar{n}_{Fj}]. \quad (8)$$

Finally, the energy density is evaluated by the Legendre transform $\mathcal{E} = \omega + T\mathcal{S} + \sum_{j=u,d} \mu_j n_j$, using the quark number density

$$n_j = \frac{N_c}{\pi^2} \int_0^\infty dp p^2 (n_{Fj} - \bar{n}_{Fj}). \quad (9)$$

In the following the evolution of matter at fixed isospin fraction $x = (n_d - n_u)/(n_u + n_d)$ is considered. Some characteristic quantities of the thermodynamical evolution of the system are the specific heat capacities $c_V = T(\partial\mathcal{S}/\partial T)_n$, $c_P = T(\partial\mathcal{S}/\partial T)_{n,P}$, the isothermal speed of sound $v_T = -(\partial\omega/\partial\mathcal{E})_{T,x}$ and the second order susceptibilities χ [41–44, 46–52]. The speed of sound is a useful indicator of the emergence of new degrees of freedom. Meanwhile the susceptibilities manifest the dynamical fluctuations characterizing the bulk (semi-classical) behavior of the system [53–55]. Fluctuations are closely related to phase transitions, in particular those related to conserved charges. For such reason the susceptibilities associated with conserved charges have been focused within the LQCD [48, 54, 55].

In the following the susceptibilities associated with the quark numbers

$$\chi_B = \left(\frac{\partial n_B}{\partial \mu_B} \right)_{\mu_3}, \quad \chi_3 = \left(\frac{\partial n_3}{\partial \mu_3} \right)_{\mu_B}, \quad \chi_{Bx} = \left(\frac{\partial n_B}{\partial \mu_B} \right)_x, \quad \chi_{3x} = \left(\frac{\partial n_3}{\partial \mu_3} \right)_x$$

will be considered. Here the densities for the baryonic number $n_B = (n_d + n_u)/3$, and the isospin number $n_3 = n_d - n_u$ have been introduced, together with the chemical potentials for the baryonic $\mu_B = 3(\mu_d + \mu_u)/2$ and the isospin $\mu_3 = \mu_d - \mu_u$ charges.

In a preliminary study [56] some alternatives to the present approach were considered. For instance in the one loop approximation, as described in [28], the mesons behave as free particles with effective masses given by Eq. (2). The grand potential receives additional contributions

$$\omega_{1\text{ loop}}(T, \mu) = \omega(T, \mu) + \frac{1}{2\beta\pi^2} \sum_{\alpha=\sigma,\pi_a,\zeta_a} \left\{ \int_0^\infty dp p^2 \log(1 - e^{-\beta E_\alpha}) - \frac{\beta}{16} \left[M_\alpha^4 \log \left(\frac{M_\alpha}{M_{0\alpha}} \right) + \frac{M_{0\alpha}^4 - M_\alpha^4}{4} \right] \right\}$$

This scheme breaks down at nonzero density because the pion mass becomes imaginary. In flavor symmetric matter it is found that $M_\pi^2 < 0$ as soon as $s/f_\pi < 0.9$, which happens at relatively low density. The problem of the imaginary meson mass at finite temperature and zero density is known from long time ago [57], and it has motivated alternatives to the ordinary loop expansion. The CJT formalism [40, 58], for instance, is efficient to treat this failure at zero density [59]. The grand potential is considered a functional of the mean values s, z and the full meson propagators, for this reason the effective masses are given by coupled self-consistent equations [39, 40, 58]. An attempt to use the CJT method within the two-flavor LSMq to describe dense systems produce similar results, but in this case both the pion and the a_0 meson masses become imaginary.

Thus I restrict here to the Hartree approach, expecting that it serves as a guide to develop an approach to dense matter including the effect of meson fluctuations.

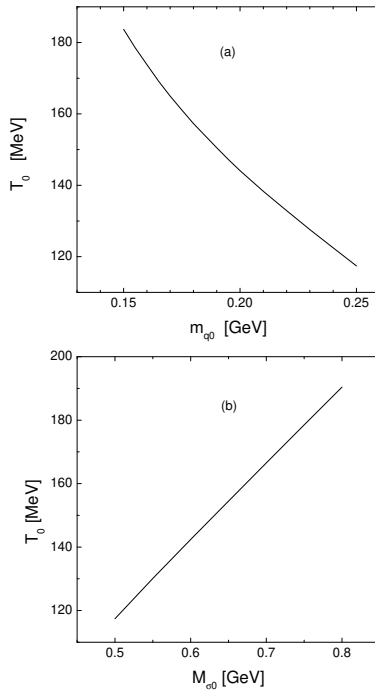


FIG. 1: The critical temperature in terms of the quark mass (a), and its dependence on the model parameter M_{σ_0} (b). The quark mass in vacuum is related to the coupling constant by $m_{q0} = g f_\pi$.

III. RESULTS AND DISCUSSION

The parameters of the model (1) are fixed in order to reproduce the physical masses of the mesons in vacuum

$$C_0 = \frac{M_{\sigma_0}^2 - 3M_{\pi_0}^2}{2}, C_2 = \frac{M_{\zeta_0}^2 - 3M_{\pi_0}^2}{2f_\pi^2}, C_3 = \frac{M_{\sigma_0}^2 - M_{\pi_0}^2}{2f_\pi^2},$$

following the standards of the model it is assumed that $s = f_\pi$ in the same conditions. Furthermore the values $M_{\sigma_0} = 500$ MeV, $M_{\pi_0} = 138$ MeV, and $M_{\zeta_0} = 984$ MeV have been used. In particular the value of M_{ζ_0} arises from the identification of the ζ meson with the $a_0(980)$, since this is the lightest manifestation in the hadronic sector of an scalar isovector. Finally, the coupling constant g is related to the quark constituent mass through $m_{q0} = g f_\pi$ and it will be discussed in the next step.

The chiral phase transition in homogeneous quark matter, keeping constant the isospin fraction, is analyzed using the model thus defined. The relation between chiral breakdown and deconfinement is not clear yet, and for the sake of simplicity it is not treated here. However, this subject has been extensively studied, specially with the aid of a phenomenological Polyakov potential. [15, 21, 48, 51, 52, 60]. Furthermore, neither the pion condensation nor the superconducting quark phase will be taken into account here since the conditions considered in this work are below the threshold of these phenomena. For instance, the isospin chemical potential verifies $\mu_3 < M_{\pi_0}$. In fact, at fixed x the chemical potential μ_3 increases with n , and for the highest density considered $n/n_0 = 5$ it is found $\mu_3/M_{\pi_0} < 0.45(0.95)$ for $x = 1/3(2/3)$ and $T \leq 20$ MeV.

There is currently a general consensus that the chiral transition is a continuous crossover for low densities and high temperatures if massive quarks are assumed. Since there is no unambiguous definition of the transition temperature in a crossover, it is defined here as the temperature of the inflection point of the chiral order parameter [61], i.e. where $s^2 + z^2$ reach its minimum value. In the present approach the critical temperature T_0 is a decreasing function of g , as shown in Fig. 1a, where a range $150 \text{ MeV} \leq m_{q0} \leq 250 \text{ MeV}$ has been considered. As can be seen, the compatibility with LQCD estimations [4] is improved adopting low values of m_{q0} . However, for such range of constituent quark masses the expected change of regime, through an intermediate CEP, is frustrated. Taking $m_{q0} = 250$ MeV the value $T_0 \simeq 120$ MeV is obtained, which is out the range $160 - 180$ MeV predicted by LQCD. This could be an effect of the parametrization used. The correlation between M_{σ_0} and the critical temperature has been studied in [36, 62], in different versions of the LSMq. An increasing dependence of T_0 with the meson mass was found there, as well as a

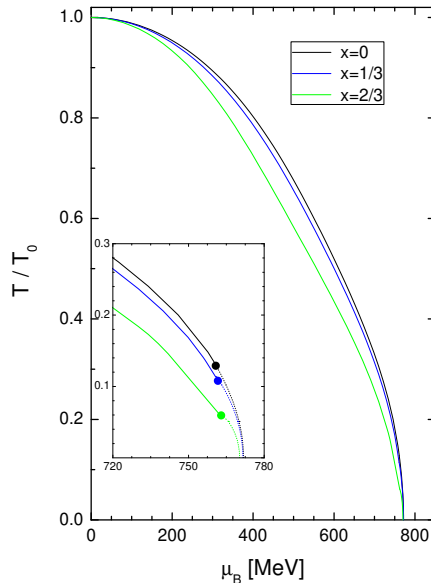


FIG. 2: The transition temperature in terms of the baryon number chemical potential for several global isospin parameters x . The insertion shows details of the first order transition (dotted lines), the CEPs (full circles) and the crossover transition (solid and dashed lines). Within the ECR the Eq.(12) applies.

decreasing trend of the CEP temperature. This relation, shown in Fig. 1b, leads to the conclusion that an increment of a few tenths of GeV for M_{σ_0} will improve the output for the critical temperature. In any case, a better fit could be obtained if higher order corrections in the meson sector are taken into account [37, 39, 63], or if the Polyakov loop potential is included [64]. A value of compromise $m_{q0} = 250$ MeV, keeping $M_{\sigma_0} = 0.5$ GeV, is adopted here to fulfill the phenomenological requirements as best as possible. Using the parametrization just described the phase diagram is evaluated for several values of x , obtaining the result shown in Fig.2. The illustrative values selected for the flavor asymmetry are as follows, $x = 0$ corresponds to the isospin symmetric case usually discussed in finite density calculations, $x = 1/3$ represents electrically neutral matter as can be found in self-bound quark stars, and finally $x = 2/3$ is an extrapolation to the negatively charged case. There is a wide variety of predictions about the position of the CEP, even using different parameterizations of the same model. An analysis of this type of uncertainty was carried out in [65] using the NJL model, concluding that the value of the chemical potential is a robust prediction of each model, while the temperature is strongly dependent on the parametrization used. In the present approach the location of the CEP changes slightly with the flavor composition. Although its chemical potential $\mu_B \simeq 770$ MeV is almost independent of x , its temperature varies within 7 – 15 MeV. Restricting the comparison for the position (μ_B, T) of the CEP to results obtained with the LSMq, one can find for instance (880,30) MeV in [37], (840,85) MeV, and (860,30) MeV in [64], and (900,30) MeV in [62]. The first case considers two flavors with two-loop mesonic corrections, the second case corresponds to 2+1 flavors with or without Polyakov potential, and the last case deals with two flavors and the octet of mesons, and parameters fixed by a specific scheme. As a general conclusion it can be stated that the present approach predicts a more reduced extension of the broken chiral phase. In addition the crossover transition temperature decreases with x for a given chemical potential μ_B .

Under certain conditions the thermodynamic potential ω does not depend monotonically on the chemical potentials or, equivalently, on the number densities. This fact is reflected by the presence of local extrema in the pressure, as exemplified in Fig.3. The isotherms for $T = 5$ MeV, corresponding to different flavor compositions, exhibit some typical situations which generate thermodynamical instabilities causing a first order phase transition. Depending on the value of the surface tension, the instabilities are resolved as a discontinuous change or as a continuous passage with an intermediate coexistence region. The last case is feasible because there are multiple conserved charges [45, 66], and both coexisting phases correspond to the regime of broken chiral symmetry. This type of transition has multiple manifestations, as in the nuclear liquid-gas transition causing the spinodal fragmentation. Assuming a low surface tension the system evolves by following the Gibbs construction. It is obtained by the introduction of a parameter λ which represents the relative abundance of the coexisting equilibrium states, named a and b in the following. Hence,

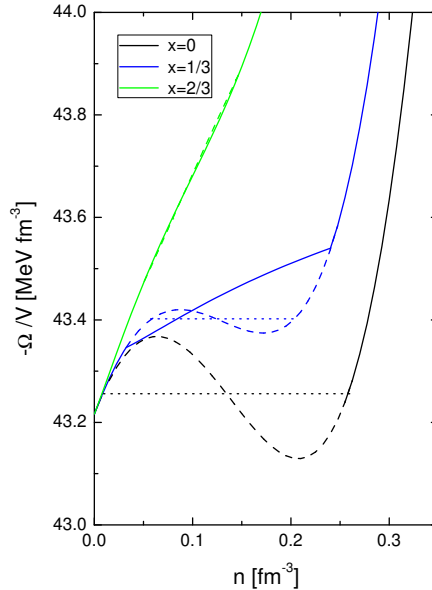


FIG. 3: The isothermal pressure at $T = 5$ MeV as function of the quark number for several flavor asymmetries x . Solid lines corresponds to the results including the ECR. The Maxwell construction for $x = 0, 1/3$ is represented by dotted lines, while the dashed lines include contributions from unstable and meta-stable configurations.

the equilibrium conditions for coexisting phases read

$$T_a = T_b, \quad \mu_B^a = \mu_B^b, \quad \mu_3^a = \mu_3^b, \quad (10)$$

$$P_a(T_a, \mu_B^a, \mu_3^a) = P_b(T_b, \mu_B^b, \mu_3^b), \quad (11)$$

while for every additive thermodynamical function one has

$$n_B = \lambda n_B^a + (1 - \lambda) n_B^b, \quad \mathcal{S} = \lambda \mathcal{S}^a + (1 - \lambda) \mathcal{S}^b, \quad \mathcal{E} = \lambda \mathcal{E}^a + (1 - \lambda) \mathcal{E}^b, \quad \text{etc.}$$

$0 \leq \lambda \leq 1$.

The curves with full lines in Fig.3 correspond to the physical situation, including the coexistence of phases through the Gibbs construction. The dotted lines represent the Maxwell construction, whose extremes are located at the onset of the metastable region. Finally, the dashed lines indicate the part of the equation of state replaced by the Gibbs construction. For $x = 0$ the Gibbs and Maxwell construction coincide since there is only one conserved charge, due to the assumption of degeneracy of the flavors u, d . The coexistence of phases extends to the $x = 2/3$ case, although there is no thermodynamical instability, and the replacement has no significant effects on the pressure. For $x = 1/3$ the parameter λ increases monotonously, exhausting its domain as the system evolves. In contrast, for $x = 2/3$, the parameter λ grows from zero to a maximum value, lesser than 1, and then returns to zero. For this reason the full and dashed lines for $x = 2/3$ almost coincide. In this situation, known as retrograde transition, the thermodynamical fluctuations are still strong, the system explores its neighborhood in the phase space, but does not find a more preferable configuration. Within the instability region, the thermodynamical potential $\omega(T, s, z, \mu_B, \mu_3)$ exhibits a non-monotonous behavior. Thus, for a given temperature one can find two different sets of variables $(s_a, z_a, \mu_{Ba}, \mu_{3a})$ and $(s_b, z_b, \mu_{Bb}, \mu_{3b})$ which reproduce the same pressure, i.e. they verify Eq.(11). If the corresponding states are coexisting, then Eq. (10) must be imposed. However such states could have very different mean field values (s_a, z_a) and (s_b, z_b) . Using Eqs. (4) and (9) one can find (n_{ua}, n_{da}) and (n_{ub}, n_{db}) or, equivalently, the quark number densities n_a, n_b and flavor asymmetries x_a, x_b for both of these states. In the following the evolution of quark matter at fixed global isospin composition x is described. Hence, this value must be kept fixed even along the coexistence region. Thus, the constraint

$$x = \frac{\lambda x_a n_a + (1 - \lambda) x_b n_b}{\lambda n_a + (1 - \lambda) n_b}. \quad (12)$$

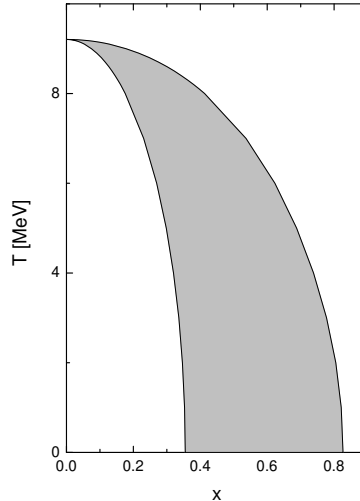


FIG. 4: An isobar section of the equilibrium coexistence region in the $x - T$ plane corresponding to $P = 45 \text{ MeV fm}^{-3}$.

must be fulfilled for coexisting phases. Inverting this relation one can find the value λ corresponding to such pair of coexisting states.

The collection of all these points, for the full range of temperatures allowed, constitutes the Equilibrium Coexistence Region (ECR). It is limited by the binodal surface and includes the part of the phase diagram originally interpreted as unstable or metastable. The ECR has been described in [67, 68] using the NJL model. To illustrate this subject an isobar section of the ECR, corresponding to $P = 43.5 \text{ MeV fm}^{-3}$, is shown in Fig. 4. It extends up to a maximum temperature $T = 9.2 \text{ MeV}$, where only states with $x_a \simeq x_b \simeq 0$ are involved. As a general trend it is found that the extension of this region reduces, until it completely disappears when *i*) the pressure increases, or *ii*) g decreases.

A correct evaluation of the derivatives involved in the definition of some bulk properties, such as heat capacity, speed of sound, etc., must take account of the dependence of the parameter $\lambda(\mu, T)$.

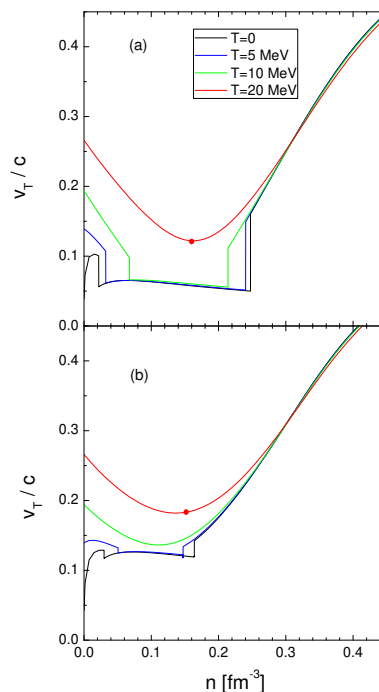


FIG. 5: The isothermal speed of sound v_T , for configurations keeping x constant, as function of the quark number density for several temperatures and $x = 1/3$ (a), and $x = 2/3$ (b). The reference density is $n_0 = 0.15 \text{ fm}^{-3}$.

The speed of sound is an important ingredient in different physical situations. The isothermal v_T as well as the adiabatic v_S speeds enter in the definition of the tidal deformability of compact stars [69], which manifests in their non-radial oscillations. For this reason it can indirectly be estimated from the analysis of the gravitational waves coming from the collapse of binary systems. This issue is under permanent attention due to the evolution of observational methods and technologies. Furthermore, it has been proposed that the high temperature behavior of v_S can be inferred from the experimental data on ultrarelativistic heavy ion collisions [70, 71]. This is in part the strong motivation for the recent studies on the speed of sound in quark matter using effective models [12, 13, 21, 27, 28, 60, 72]. Some of them explore the limit $\mu_B \rightarrow 0$ in order to contrast with LQCD results, and others extend to finite densities as for example the recent study of the relation between the speed of sound and the CEP [72].

The isothermal speed of sound, along curves at constant x , is shown in Fig.5 as a function of the quark number density for two isospin compositions and a range of n and T compatible with the first-order transition. For $x = 1/3$ (upper panel) and a temperature above the CEP, $T = 20$ MeV, the speed v_T has a non-monotonic trend with its minimum located approximately at the transition point (filled circle). For lower temperatures the system experiences the coexistence of phases, reflected by a discontinuous drop to a lower plateau. The vertical segments at the discontinuities have the sole purpose of facilitating the interpretation of the curves. Along the ECR, the speed of sound has a mild variation with the particle number, and it is approximately independent of the temperature. Furthermore, the extension of the ECR is reduced as T grows, a fact that manifests by the shrinking of the plateau. A similar description applies to $x = 2/3$ (Fig. 5b), but in such case only the isotherms corresponding to $T = 0$, and 5 MeV undergo a first order transition.

The effects of the chiral transition on the number susceptibilities have been discussed previously within the NJL model [41–43, 67], and also within the LSMq [44, 49–52]. The presence of states out of thermodynamical equilibrium has been particularly analyzed in [42, 43]. Different definitions of the susceptibilities are shown in the following two figures, as functions of the quark density for several temperatures within the range of the first order transition. For the susceptibilities associated with the baryon number, χ_B (Fig.6) and χ_{Bx} (Fig.7), strong oscillations are found at the borders of the ECR. For higher densities all the curves decay and reach quickly the asymptotic regime. In fact χ_B and χ_{Bx} coincide for $w = 0$, $T = 0$.

For $x = 0$ (Figs. 6a, and 7a) all the curves diverge at the boundaries of the unstable section of the equation of state, taking opposite signs on both sides. The same behavior was reported and discussed in [42, 43] for calculations using the NJL model.

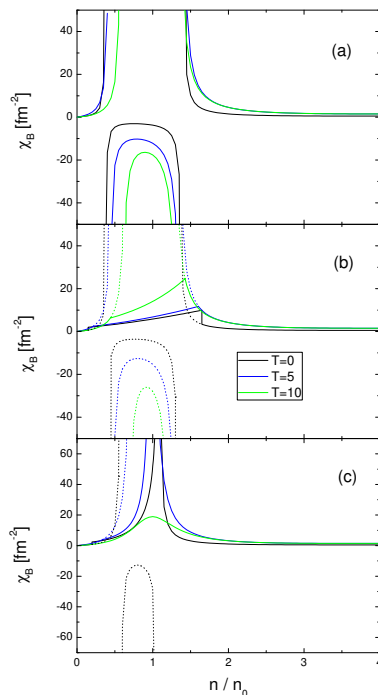


FIG. 6: The second order susceptibility corresponding to the baryonic number as function of the quark number density for several temperatures and $x = 0$ (a), $x = 1/3$ (b), and $x = 2/3$ (c). For $x = 0$ only the results using the unstable equation of state are shown. In the panels b and c the solid lines correspond to the result including the ECR, dotted lines represent the result with contributions from unstable and metastable configurations. The reference density is $n_0 = 0.15 \text{ fm}^{-3}$.

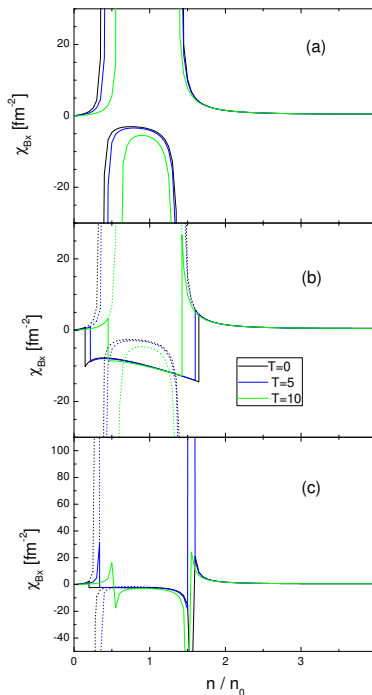


FIG. 7: The second order susceptibility corresponding to the baryonic number (keeping constant the isospin fraction) as function of the quark number density for several temperatures and $x = 0$ (a), $x = 1/3$ (b), and $x = 2/3$ (c). For $x = 0$ only the results using the unstable equation of state are shown. In the panels b and c the solid lines correspond to the result including the ECR, dotted lines represent the result with contributions from unstable and metastable configurations. The reference density is $n_0 = 0.15 \text{ fm}^{-3}$.

For $x > 0$ the contributions of the unstable region are distinguished by using dashed lines, while the results coming from the ECR are represented by solid lines. The effect of the Gibbs procedure is clear for $x = 1/3$ (Figs. 6b and 7b), where the divergences are replaced by smooth curves with finite discontinuities at the end points. In between χ_B remains positive and increasing with the density, a fact that is emphasized as the temperature grows. On the contrary, χ_{Bx} experiences a drop in the ECR and seems insensitive to the temperature.

Qualitative changes occur for the higher asymmetry $x = 2/3$. For $T = 10$ MeV the system is above the CEP and χ_B shows a regular behavior, while χ_{Bx} still shows two peaks as a remainder of the active thermodynamical fluctuations. For lower temperatures $T = 0$, and 5 MeV, both susceptibilities have large but finite discontinuities within the ECR. However it must be bear in mind that this is an extrapolation, since the effect of the weak forces will not be negligible for $x = 2/3$.

The susceptibilities associated with the isospin composition are presented in Figs. 8 and 9 as functions of the quark number density and several temperatures. The behavior of χ_3 for symmetric matter is completely regular despite the presence of the binodal. The same applies to χ_{3x} for all the cases shown in Fig. 9, and is the transition through the ECR the responsible of the discontinuities and an almost linear increase with the quark number, independently of the temperature.

As the next step the specific heat capacities are considered in Fig.10. Both the constant volume and isobar quantities are displayed for isospin asymmetric matter, showing the results coming from the ECR only. The smooth variation of c_V within the binodal was discussed in [43]. In the present case finite discontinuities are found at the extremes of the ECR which do not affect significantly the general increasing trend. The isobaric counterpart c_P exhibits a more interesting behavior, a strong dependence on x is shown either in the crossover regime ($T = 20$ MeV) or near the CEP ($T = 10$ MeV). In the last case a drop to $c_P < 0$ occurs within the ECR. Such unexpected result has also been found in nuclear physics and considered as a signal of the liquid-gas transition [73–75]. The curves for $x = 1/3$ show drastic thermal effects around the CEP, as it is evident by comparing the $T = 20$ MeV and $T = 10$ MeV cases. This effect becomes extreme for the higher asymmetry $x = 2/3$ and temperatures $T = 5 - 10$ MeV, passing from a smooth dependence to a negative peak concentrated at the border of the ECR.

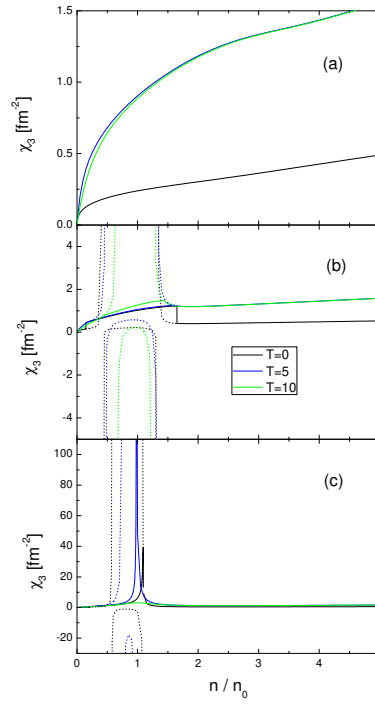


FIG. 8: The second order susceptibility corresponding to the isospin number as function of the quark number density for several temperatures and $x = 0$ (a), $x = 1/3$ (b), and $x = 2/3$ (c). For $x = 0$ only the results using the unstable equation of state are shown. In the panels b and c the solid lines correspond to the result including the ECR, dotted lines represent the result with contributions from unstable and metastable configurations. The reference density is $n_0 = 0.15 \text{ fm}^{-3}$.

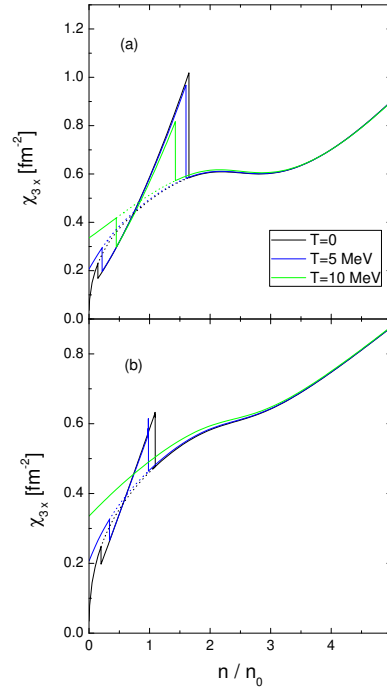


FIG. 9: The second order susceptibility corresponding to the isospin number (keeping constant the isospin fraction) as function of the quark number density for several temperatures and $x = 1/3$ (a), and $x = 2/3$ (b). Solid lines correspond to the result including the ECR, dotted lines represent the result with contributions from unstable and metastable configurations. The reference density is $n_0 = 0.15 \text{ fm}^{-3}$.

IV. SUMMARY AND CONCLUSIONS

In this work the chiral phase transition of homogeneous quark matter, assuming the conservation of both baryonic and isospin numbers, has been studied. This subject has been intensively studied in recent years, motivated in part by the availability of LQCD calculations, which overcame technical difficulties in the limit of zero baryon density. Thus, investigations using effective models have found a source of reliable data to contrast with their predictions and an opportunity to improve their frameworks. Since LQCD is efficient in the limit of zero baryonic density, much of the recent theoretical efforts have scrutinized such regime [2, 20, 22–24, 27, 28]. The chiral transition at non-zero baryonic density is still the domain of theoretical speculation by using effective models. Interesting effects have been pointed out, such as the manifestations of thermodynamical fluctuations near the non-equilibrium region of the first order phase transition [41–44, 49]. By definition this domain can not be analyzed by the equilibrium thermodynamics. However, if multiple charges are conserved and a low surface tension is assumed, the system could undergo a continuous transition through the coexistence of equilibrium states [45, 66]. The LSMq with two flavors has been used here to explore this hypothesis, introducing the scalar isovector meson ζ as a necessary element to take account of isospin imbalanced quark matter at finite density. The calculations have been performed in the MFA with vacuum contributions of the quark sector. The analysis of the effects of higher order mesonic corrections to this scheme is in progress. Neither pion condensation nor quark superconductivity have been considered since the chemical potentials μ_B , μ_3 are below the corresponding thresholds for the range of this calculation.

The assumptions made in the present approach, as well as the range of variables considered, make these results more appropriate for astrophysical situations, as for instance the structure and dynamics of self-bound stars [69].

The phase diagram obtained here is in qualitative agreement with present knowledge, a smooth crossover at high temperatures ends at a CEP, and changes to a first order transition at low temperatures. Although the value obtained for the critical temperature is too low, it is expected that higher order mesonic corrections will improve this result [37, 39, 63]. The transition lines for several isospin asymmetries have been obtained, showing that along the crossover the transition temperature decreases slightly with increasing the isospin asymmetry x . The first-order transition occurs as a continuous succession of equilibrium states obtained by the Gibbs construction.

The equation of state as well as several bulk properties of quark matter exhibit important modifications through the ECR. In the crossover regime, the isothermal speed of sound at constant $x > 0$ has a non-monotonic dependence on the particle density. It presents a minimum in coincidence with the transition point. Within the coexistence region

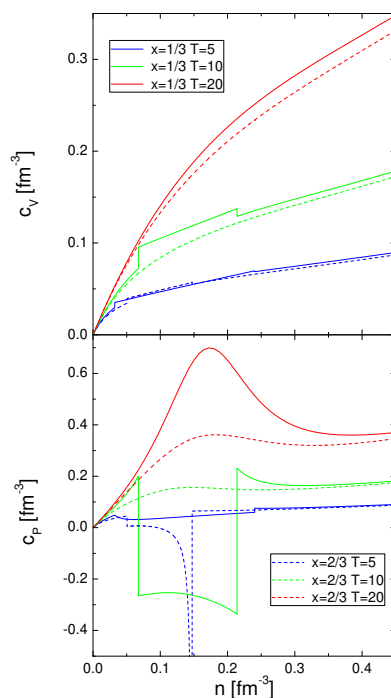


FIG. 10: The specific heat at constant volume (a) and at constant temperature (b) as functions of the quark number density for the asymmetries $x = 1/3, 2/3$, and temperatures $T = 5, 10, 20$ MeV. The line convention is presented in two separate tables, one on each panel.

the speed v_T experiences a noticeable decrease with finite discontinuities at the borders. A mild variation of v_T with density and temperature is predicted for this domain.

The susceptibility associated with the baryonic number, both using the standard definition (χ_B) as well as that keeping x constant (χ_{Bx}), remain bounded along the ECR for low asymmetry parameter $x > 0$. This result contrast with calculations using the unstable sector of the equation of state. A distinctive difference is that χ_B remains positive inside the ECR. As x grows, large but finite discontinuities appear at the high density border of the ECR.

A similar description applies to χ_3 , with the noticeable difference that for $x = 0$ it remains bounded as predicted in previous calculations [41]. However the presence of the binodal has clear manifestations for $x > 0$.

In regard of the specific heat c_V , only small deviations from the continuous behavior are introduced by the ECR. The isobaric counterpart c_P takes unexpected negative values, a fact known in nuclear physics and interpreted as a signal of the spinodal fragmentation [73–75].

Acknowledgements

This work has been partially supported by CONICET, Argentina under the project 11220200102081CO, and by UNLP, Argentina.

Appendix A

The vacuum contribution to the grand potential has been discussed in numerous works. In particular it has been pointed out [50], that its inclusion in the two flavor LSMq changes the character of the chiral transition. For the sake of completeness, the deduction of Eq.(5) is shown in the following.

The contribution of the Dirac sea to the thermodynamical potential, see for instance [38], is given by

$$\omega_{\text{vac}} = -2N_c \sum_{j=u,d} \int \frac{d^3p}{(2\pi)^3} E_j, \quad (\text{A1})$$

where $E_j^2 = p^2 + m_j^2$, and the integral is clearly ultraviolet divergent. However, the divergence can be expressed as an isolated pole using dimensional regularization. For this purpose the integral is rewritten in terms of the causal Dirac propagator as

$$I_j = \int \frac{d^3p}{(2\pi)^3} E_j = 2i \int \frac{d^4p}{(2\pi)^4} \frac{p_0^2}{p_0^2 - E_j^2 + i\epsilon} = \lim_{\epsilon \rightarrow 0} 2i \int \frac{d^d p}{(2\pi)^d} \frac{p_\mu p^\nu}{(p_0^2 - E_j^2)^\alpha}.$$

On the right hand side the integration is carried out in a space of dimension $d = 4 - 2\epsilon$, and $\mu = \nu = 0$, $\alpha = 1$. This is a typical expression which can be found in several texts, leading to the result

$$I_j = \left(\frac{m_j^2}{4\pi} \right)^2 \lim_{\epsilon \rightarrow 0} (m_j^2)^{-\epsilon} \Gamma(\epsilon - 2) = \frac{m_j^4}{32\pi^2} \lim_{\epsilon \rightarrow 0} \left[\frac{1}{\epsilon} + \frac{3}{2} - \gamma - \ln(m_j^2) + \mathcal{O}(\epsilon) \right].$$

In the right hand side the divergence appears as a simple pole at $\epsilon = 0$ with main coefficient $m_j^2/32\pi^2$. For this reason one can define a regularized integral by taking the reference state with zero density and temperature, where the quark mass is degenerate $m_j = m_0$, and applying a subtraction scheme

$$\begin{aligned} I_j^{\text{reg}} &= I_j - I_j(m_j = m_0) - (m_j^4 - m_0^4) \frac{dI_j}{dy}(m_j = m_0) \\ &= \frac{1}{64\pi^2} \left[m_j^4 - m_0^4 - m_j^4 \ln \left(\frac{m_j^4}{m_0^4} \right) \right] \end{aligned}$$

where $y = m_j^4$. Thus the regularized contribution from the quark Dirac sea is

$$\omega_{\text{vac}} = \frac{N_c}{32\pi^2} \sum_{j=u,d} \left[m_0^4 - m_j^4 + m_j^4 \ln \left(\frac{m_j^4}{m_0^4} \right) \right] \quad (\text{A2})$$

-
- [1] M. G. Alford, A. Kapustin, and F. Wilczek, *Phys. Rev. D* **59**, 054502 (1999).
- [2] D. T. Son and M. A. Stephanov, *Phys. Rev. Lett.* **86**, 592 (2001).
- [3] Y. Nishida, *Phys. Rev. D* **69**, 094501 (2004).
- [4] S. Ejiri, Y. Maezawa, N. Ukita, S. Aoki, T. Hatsuda, N. Ishii, K. Kanaya, and T. Umeda (WHOT-QCD), *Phys. Rev. D* **82**, 014508 (2010).
- [5] K. Aryal, C. Constantinou, R. L. S. Farias, and V. Dexheimer, *Phys. Rev. D* **102**, 076016 (2020).
- [6] A. Prakash, I. Gupta, M. Breschi, R. Kashyap, D. Radice, S. Bernuzzi, D. Logoteta, and B. S. Sathyaprakash, *Phys. Rev. D* **109**, 103008 (2024).
- [7] D. Toublan and J. B. Kogut, *Phys. Lett. B* **564**, 212 (2003).
- [8] M. Frank, M. Buballa, and M. Oertel, *Phys. Lett. B* **562**, 221 (2003).
- [9] A. Barducci, R. Casalbuoni, G. Pettini, and L. Ravagli, *Phys. Rev. D* **69**, 096004 (2004).
- [10] A. Barducci, G. Pettini, L. Ravagli, and R. Casalbuoni, *Phys. Lett. B* **564**, 217 (2003).
- [11] M. Loewe and C. Villavicencio, *Phys. Rev. D* **71**, 094001 (2005).
- [12] L.-y. He, M. Jin, and P.-f. Zhuang, *Phys. Rev. D* **71**, 116001 (2005).
- [13] L. He and P. Zhuang, *Phys. Lett. B* **615**, 93 (2005).
- [14] Z. Zhang and Y.-x. Liu, *Phys. Rev. C* **75**, 035201 (2007).
- [15] S. Mukherjee, M. G. Mustafa, and R. Ray, *Phys. Rev. D* **75**, 094015 (2007).
- [16] P. Kovacs and Z. Szep, *Phys. Rev. D* **77**, 065016 (2008).
- [17] C.-f. Mu, L.-y. He, and Y.-x. Liu, *Phys. Rev. D* **82**, 056006 (2010).
- [18] H. Abuki, *Phys. Rev. D* **87**, 094006 (2013).
- [19] T. Xia, L. He, and P. Zhuang, *Phys. Rev. D* **88**, 056013 (2013).
- [20] R. Stiele, E. S. Fraga, and J. Schaffner-Bielich, *Phys. Lett. B* **729**, 72 (2014).
- [21] H. Liu, J. Xu, L.-W. Chen, and K.-J. Sun, *Phys. Rev. D* **94**, 065032 (2016).
- [22] S. S. Avancini, A. Bandyopadhyay, D. C. Duarte, and R. L. S. Farias, *Phys. Rev. D* **100**, 116002 (2019).
- [23] B. S. Lopes, S. S. Avancini, A. Bandyopadhyay, D. C. Duarte, and R. L. S. Farias, *Phys. Rev. D* **103**, 076023 (2021).
- [24] P. Adhikari and J. O. Andersen, *Physics Letters B* **804**, 135352 (2020).
- [25] P. Costa, R. Câmara Pereira, and C. Providência, *Phys. Rev. D* **102**, 054010 (2020).
- [26] P.-C. Chu, X.-H. Li, H. Liu, M. Ju, and Y. Zhou, *Phys. Rev. C* **108**, 025808 (2023).
- [27] A. Ayala, A. Bandyopadhyay, R. L. S. Farias, L. A. Hernández, and J. L. Hernández, *Phys. Rev. D* **107**, 074027 (2023).
- [28] A. Ayala, B. S. Lopes, R. L. S. Farias, and L. C. Parra, *Phys. Lett. B* **864**, 139396 (2025).
- [29] S. K. Ghosh, A. Lahiri, S. Majumder, M. G. Mustafa, S. Raha, and R. Ray, *Phys. Rev. D* **90**, 054030 (2014).
- [30] D. Parganlija, F. Giacosa, and D. H. Rischke, *Phys. Rev. D* **82**, 054024 (2010).
- [31] D. Parganlija, P. Kovacs, G. Wolf, F. Giacosa, and D. H. Rischke, *Phys. Rev. D* **87**, 014011 (2013).
- [32] P. Kovács, Z. Szép, and G. Wolf, *Phys. Rev. D* **93**, 114014 (2016).
- [33] S. Gasiorowicz and D. A. Geffen, *Rev. Mod. Phys.* **41**, 531 (1969).
- [34] D. Metzger, H. Meyer-Ortmanns, and H. J. Pirner, *Phys. Lett. B* **321**, 66 (1994), [Erratum: *Phys.Lett.B* 328, 547–547 (1994)].
- [35] J. T. Lenaghan, D. H. Rischke, and J. Schaffner-Bielich, *Phys. Rev. D* **62**, 085008 (2000).
- [36] B.-J. Schaefer and M. Wagner, *Phys. Rev. D* **79**, 014018 (2009).
- [37] A. Ayala, L. A. Hernández, M. Loewe, J. C. Rojas, and R. Zamora, *Eur. Phys. J. A* **56**, 71 (2020).
- [38] L. Dolan and R. Jackiw, *Phys. Rev. D* **9**, 3320 (1974).
- [39] N. Petropoulos, *J. Phys. G* **25**, 2225 (1999).
- [40] J. M. Cornwall, R. Jackiw, and E. Tomboulis, *Phys. Rev. D* **10**, 2428 (1974).
- [41] C. Sasaki, B. Friman, and K. Redlich, *Phys. Rev. D* **75**, 054026 (2007).
- [42] C. Sasaki, B. Friman, and K. Redlich, *Phys. Rev. Lett.* **99**, 232301 (2007).
- [43] C. Sasaki, B. Friman, and K. Redlich, *Phys. Rev. D* **77**, 034024 (2008).
- [44] B. Stokic, B. Friman, and K. Redlich, *Phys. Lett. B* **673**, 192 (2009).
- [45] N. K. Glendenning, *Phys. Rev. D* **46**, 1274 (1992).
- [46] R. V. Gavai and S. Gupta, *Phys. Rev. D* **64**, 074506 (2001).
- [47] L. Ferroni and V. Koch, *Phys. Rev. C* **83**, 045205 (2011).
- [48] C. Ratti, S. Roessner, and W. Weise, *Phys. Lett. B* **649**, 57 (2007).
- [49] G. A. Almasi, B. Friman, and K. Redlich, *Phys. Rev. D* **96**, 014027 (2017).
- [50] V. Skokov, B. Friman, E. Nakano, K. Redlich, and B. J. Schaefer, *Phys. Rev. D* **82**, 034029 (2010).
- [51] V. Skokov, B. Stokic, B. Friman, and K. Redlich, *Phys. Rev. C* **82**, 015206 (2010).
- [52] V. Skokov, B. Friman, and K. Redlich, *Phys. Rev. C* **83**, 054904 (2011).
- [53] M. Asakawa, U. W. Heinz, and B. Muller, *Phys. Rev. Lett.* **85**, 2072 (2000).
- [54] R. V. Gavai and S. Gupta, *Phys. Rev. D* **73**, 014004 (2006).
- [55] S. Datta, R. V. Gavai, and S. Gupta, *Phys. Rev. D* **95**, 054512 (2017).
- [56] R. M. Aguirre, arXiv preprint nucl-th/2511.11822 (2025).
- [57] H. Goldberg, *Phys. Lett. B* **131**, 133 (1983).
- [58] G. Amelino-Camelia and S.-Y. Pi, *Phys. Rev. D* **47**, 2356 (1993).

- [59] D. Roder, J. Ruppert, and D. H. Rischke, *Phys. Rev. D* **68**, 016003 (2003).
- [60] S. K. Ghosh, T. K. Mukherjee, M. G. Mustafa, and R. Ray, *Phys. Rev. D* **73**, 114007 (2006).
- [61] J. M. Pawłowski and F. Rennecke, *Phys. Rev. D* **90**, 076002 (2014).
- [62] S. K. Rai and V. K. Tiwari, *Phys. Rev. D* **105**, 094010 (2022).
- [63] N. Bilic and H. Nikolic, *Eur. Phys. J. C* **6**, 515 (1999).
- [64] B.-J. Schaefer and M. Wagner, *Phys. Rev. D* **85**, 034027 (2012).
- [65] A. Biguet, H. Hansen, T. Brugière, P. Costa, and P. Borgnat, *Eur. Phys. J. A* **51**, 121 (2015).
- [66] H. Heiselberg and M. Hjorth-Jensen, *Phys. Rept.* **328**, 237 (2000).
- [67] P. Costa, M. C. Ruivo, and C. A. de Sousa, *Phys. Rev. D* **77**, 096001 (2008).
- [68] L.-M. Liu, W.-H. Zhou, J. Xu, and G.-X. Peng, *Phys. Lett. B* **822**, 136694 (2021), 2104.12971.
- [69] A. Zacchi and J. Schaffner-Bielich, *Phys. Rev. D* **100**, 123024 (2019).
- [70] F. G. Gardim, G. Giacalone, M. Luzum, and J.-Y. Ollitrault, *Nature Phys.* **16**, 615 (2020).
- [71] Y.-S. Mu, J.-A. Sun, L. Yan, and X.-G. Huang, *Phys. Rev. Lett.* **135**, 162301 (2025).
- [72] S. Hernández-Ortiz, R. M. von Dossow, and A. Raya, *Eur. Phys. J. A* **60**, 154 (2024).
- [73] M. D'Agostino et al., *Phys. Lett. B* **473**, 219 (2000).
- [74] B. Borderie et al., *Eur. Phys. J. A* **56**, 101 (2020).
- [75] J. N. De, S. K. Samaddar, S. Shlomo, and J. B. Natowitz, *Phys. Rev. C* **73**, 034602 (2006).